Toward the Ultimate Limit of Connectivity in Quantum Dots with High Mobility and Clean Gaps

Huashan Li,[†,‡] David Zhitomirsky,[†,‡] Shreya Dave,[†,§] and Jeffrey C. Grossman*,[†]

[†]Department of Materials Science and Engineering and [§]Department of Mechanical Engineering, Massachusetts Institute of Technology, Cambridge, Massachusetts 02139, United States

S *Supporting Information*

ABSTRACT: Colloidal quantum dots (CQDs) are highly versatile nanoscale optoelectronic building blocks, but despite their materials engineering flexibility, there is a considerable lack of fundamental understanding of their electronic structure as they couple within thin films. By employing a joint experimental−theoretical study, we reveal the impact of connectivity in CQD assemblies, going beyond the single CQD picture. High-resolution transmission electron microscopy (HR-TEM) demonstrates connectivity motifs across different CQD sizes and length scales and provides the necessary perspective to build robust computational models to systematically study the achievable degree of connectivity in

these materials. We focused on state-of-the-art surface ligand treatments, taking into account both the degree of connectivity and nanocrystal orientation, and performed *ab initio* simulations within the phonon-assisted hopping regime. Importantly, both the TEM studies and our simulation results revealed morphological and electronic defects that could dramatically reduce optoelectronic performance, and yet would not have been captured within a single CQD model that neglects connectivity. We calculate carrier mobility in the presence of such defect states and conclude that the best-achievable CQD assemblies for optoelectronics will require a modest degree of fusing *via* the {001} facet, followed by atomic ligand passivation to generate a clean band gap and unprecedentedly high charge transport.

KEYWORDS: *colloidal QD, charge transport, necking, high-resolution TEM, density functional theory*
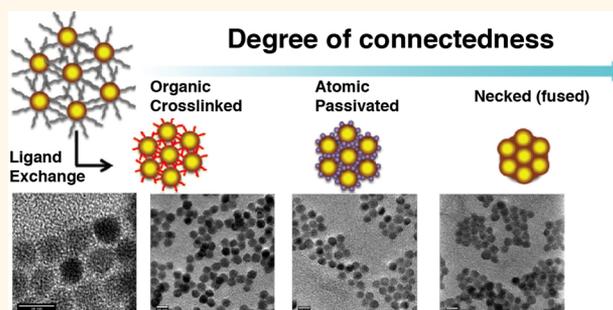
O f the various types of nanomaterials, colloidal quantum dots (CQDs) are especially promising for commercial electronic and optoelectronic applications due to their band gap tunability, high photostability, inexpensive solution processing, large-scale manufacturing, and compatibility with flexible substrates.[1]

Two major classes of approaches have been developed to optimize the CQD-based devices. One focuses on designing functionalization to eliminate trap states[2−7] and to tune the doping levels of each dot.[8,9] Record-high performance of CQD-based solar cells has been achieved by hybrid functionalization schemes,[2−4] and stoichiometry control *via* ligand modification[8] or atomic infusion[9] has enabled both n- and p-type CQD thin films.

The other approach focuses on enhancing carrier mobility by designing connectivity between CQDs with either bridging (connected by ligands) or necking (fused, without a ligand). While atomic bridges like TBAI[10] and bidentate bridges such as EDT,[11] MPA,[2] and molecular metal chalcogenide ligands,[12] have been employed to improve carrier mobilities by orders of magnitude compared to longer ligands, it was only recently that

another remarkable improvement was obtained in confined but connected CQDs.[13−16] The attachment orientation of such necked CQDs could even be controlled by temperature and particle concentration to form various types of supperlattices.[13−15]

While the design strategy for the functionalization of CQDs has been extensively explored by employing multiscale simulations,[17,18] no systematic study has been carried out to clarify the optimization strategy for connectivity. Such a knowledge gap may originate from the difficulties in high-resolution imaging of small CQDs as well as development of a theoretical model that captures effects arising from the irregularly connected nature of CQD films containing defects. To fulfill the potential of CQD-based optoelectronic applications, we must address this gap *via* combined experimental and theoretical efforts to provide comprehensive
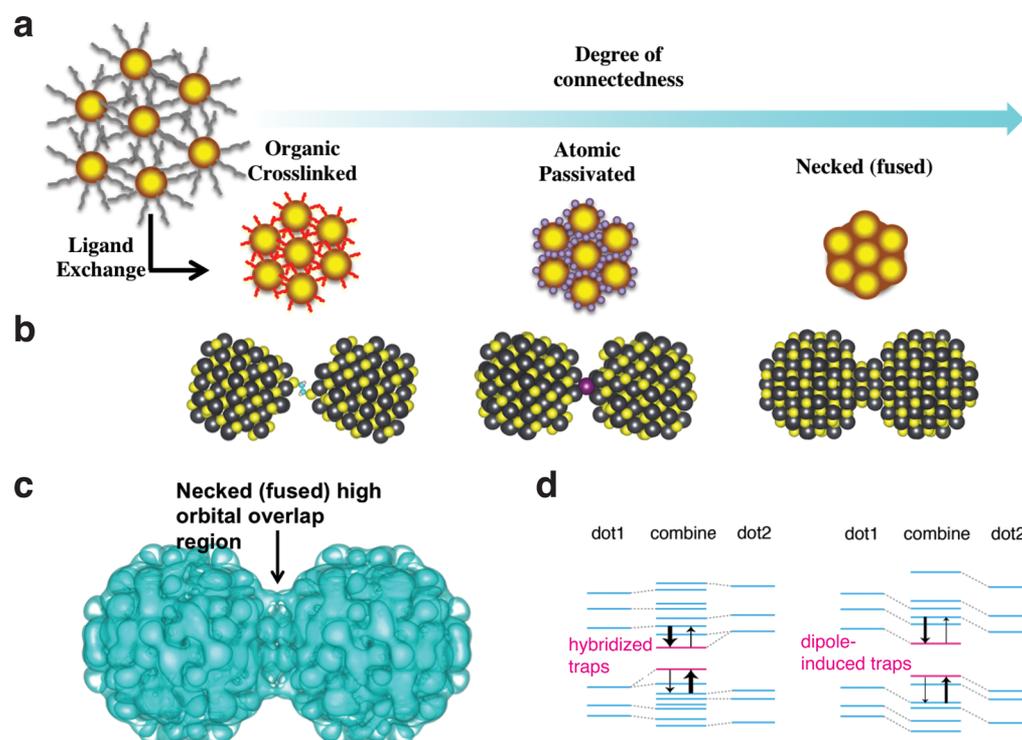
Figure 1. Impact of CQD communication. (a) Illustrations of the ligand exchange procedure leading to varying degrees of connectivity between CQDs. (b) Atomic structure of PbS CQDs that are connected with organic (ethane dithiol, left) and inorganic (iodine, middle) ligands, as well as necked (fused, right) CQDs expected to result in high mobility. (c) Calculated orbital overlaps on necked CQD structures exhibiting high overlap in the region between the CQDs. (d) Hybridization and dipole-induced trap states arising directly from connectivity between CQDs.

understanding of morphological and electronic properties on both device and atomic scales. In particular, given the strong electron coupling and precise control of connectivity attainable by emerging film-processing techniques,[13−15] it is imperative to understand the way in which connectivity between CQDs affects the behavior of the entire system and whether the configuration of connectivity could serve as a new degree of control to optimize device performance.

In this work, we employ two different sizes of CQD and study the impact of a variety of standard ligands in order to achieve variable degrees of connectivity, including the cases of necking (where the CQDs are fused together) without ligand and bridging (where the CQDs are connected but remain separate and unfused) by ligands as illustrated in Figure 1a,b. These results reveal unexpected effects that could manifest as energy defects in a device, which could impede carrier transport in large-scale assemblies. Motivated by our experimental findings and using them as a basis, accurate quantum mechanical methods were employed to analyze the energy levels and carrier mobilities of PbS CQDs. Our results suggest that accounting for interactions between irregularly connected dots is necessary to understand the characteristics of CQD assemblies. First, for comparatively small dots, we show that bridging by small molecules may introduce trap states due to orbital hybridization and a dipole-induced potential drop (Figure 1d). Second, our calculations indicate that carrier mobility varies by orders of magnitude with different bridges, orientations, carrier energies, and defect levels (Figure 1c). On the basis of these observations, we provide guidelines for designing connectivity to improve device performance further.

RESULTS AND DISCUSSION

Experimental evidence has effectively provided context for broader theoretical design of these materials, enabling control over electronic doping,[17,18] band alignment,[19] and trap state models.[2] We used high-resolution transmission electron microscopy (HR-TEM) to directly observe the degree of connectivity between CQDs in order to reveal broader design principles for making CQD solids with superior optoelectronic properties.

We fabricated CQD films using three classes of ligands that have been widely reported in the PbS CQD literature and offer an increasing degree of connectivity evaluated based on GISAXS measurements[20] in order to study the resultant morphology and film formation behavior. To better capture the impact of ligand connectivity on CQD size, we have employed two types of CQDs with a significant size difference (3 and 8 nm, absorption spectra in Supplementary Figure S1). We find that ligand exchange behavior as a function of CQD size can result in dramatic morphological variations that in turn alter the CQD solid energetic landscape, thus mandating redesign of the exchange procedure. Additionally, employing differently sized CQDs enables extrapolating different ligand effects that are difficult to discern at very low CQD sizes (<3 nm).

PbS CQDs of 3 nm are materials predominantly employed in photovoltaic (PV) applications. Reports on imaging films made from these particles remain sparse due to low contrast in TEM and complex morphologies arising from ligand exchange, hence requiring a combined study alongside larger particles to shed light on the phenomena occurring at the smaller scale. The right choice of CQD concentration, solvent drying technique, and purification is critical to achieve informative and repeatable

images where individual particles may be resolved (methods). An important ligand for photovoltaic fabrication is tetrabutylammonium iodide (TBAI), typically used in concentrations of 10−20 mg/mL;[21,22] we chose this ligand along with methanol as solvent and adjusted the concentrations and solvent for all other ligands accordingly. Figure 2a depicts as-synthesized 3
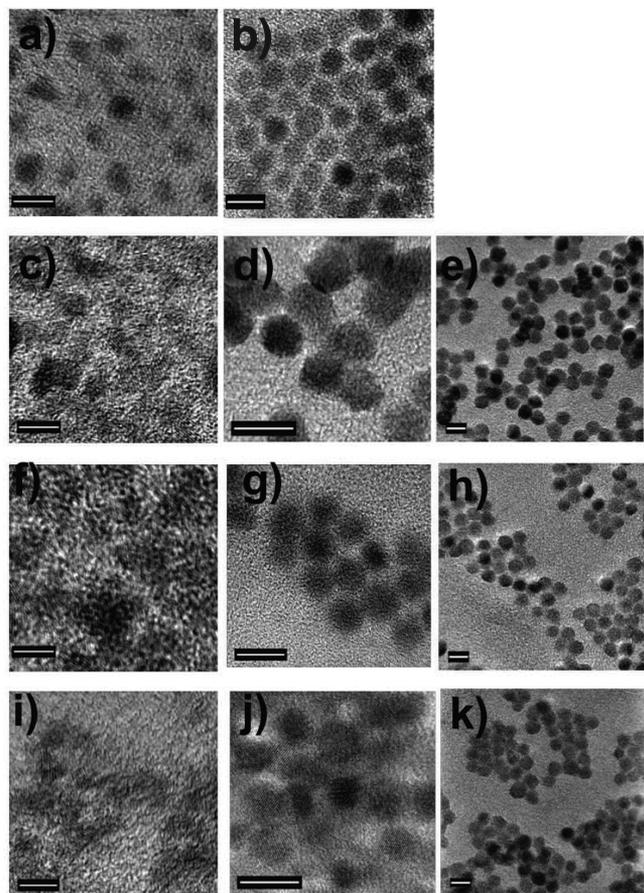
Figure 2. (a) 3 nm and (b) 8 nm control PbS CQD samples. (c) 3 nm CQDs treated with 0.05 M EDT in MeOH. (d) Microscale and (e) macroscale 8 nm CQDs treated with EDT. (f) 3 nm CQDs treated with atomic spacers using a 0.05 M TBAI salt in MeOH. (g) Microscale and (h) macroscale images of the same treatment on 8 nm particles. (i) 3 nm CQD particles treated with EDA to achieve partial CQD necking (fusing). (j) Microscale and (k) macroscale images of 8 nm particles with the same treatments. Scale bars are 5 nm for 3 nm CQDs and 10 nm for 8 nm CQDs.

nm particles separated by long and insulating oleic acid (OA) ligands. The high-resolution images show clearly crystal structures in focus for dots at the same Z-height. Because the film is not perfectly flat, further complexity is introduced in resolving all dots in an image to the same degree. Upon ligand exchange with an ethane dithiol (EDT) organic linker (Figure 2c), the nanocrystals form clusters, where it is possible that both bridging and necking (fusing) may be occurring. We independently verify that methanol itself does not cause necking of the nanocrystals (Supplementary Figure S2). Upon using the same ligand with the large 8 nm, IR-communications-relevant PbS CQDs (Figure 2d), the CQD spacing is reduced with EDT compared to the OA case (Figure 2b), and macroscale order is not preserved (Figure 2e); however, it does not appear the nanocrystals form fused

structures. Additionally, the particles may often be seen to be overlapping, suggesting they migrate to different planes relative to one another, thus limiting potential for ordering important for electronic transport in superlattices.

The use of a TBAI salt as a source of iodine atomic linker[21] (Figure 2f) results in similar morphological changes for the 3 nm particles to the EDT case, but also in rare large agglomerates not present in our control samples with consistent lattice spacing, suggestive of fused clusters (Supplementary Figure S3), which were not observed in any of our EDT samples, and suggests that PbS CQDs may be susceptible to fusing due to halogens displacing atoms from the core of the particle, as has been reported in work on CQD electronic doping[18,21] and is known for the bulk material. However, absorption spectra of a layer-by-layer TBAI film showed a clear excitonic peak, indicating that macroscale fusing had not occurred (Supplementary Figure S4). Treating 8 nm CQDs with these ligands shows, in addition to increased connectivity compared to the OA case (Figure 2g), a better preserved macroscopic order (Figure 2h), where a more detailed comparison is given in the Supporting Information (Figure S5 and Table S5). Such preservation of macroscopic order compared to the EDT case may arise due to TBAI's propensity to make weaker bonds to the nanocrystal surface than EDT, thus enabling the nanocrystals to experience a more controlled ligand exchange and settle into energetically favorable configurations.

In order to achieve yet another increase in connectivity, we have employed recently reported diamine ligands (ethyl diamine, EDA); these ligands strip away lead oleate in PbSe CQDs, thus exposing a bare CQD surface that is capable of interacting with neighboring nanocrystals.[13] For 3 nm PbS particles (Figure 2i), it appears that some degree of fusing may be occurring, as structures resemble continuous chains of connected nanoparticles. To investigate this effect further, we employed a ligand exchange an order of magnitude higher in concentration (∼1 M), which revealed apparent total fusing of these small crystals into larger agglomerates (Supplementary Figure S6). As before, the difference in this treatment compared to EDT and TBAI can be clearly seen for large CQDs (Figure 2j), where there is increased clustering and multiple particles appear to have fused together. Although several works have reported fused particles where consistent fringe patterns are seen across the junction,[13,23] it remains unclear whether that is a necessary condition for necking, as this phenomenon can in principle occur between different types of facets and with varying degrees of fusing. In the macroscopic image (Figure 2k), a consistent effect of edge fusing for neighboring CQDs is much more prominent than for either the EDT or TBAI treatment. Treating these CQDs with a higher concentration of EDA (Supplementary Figure S7) resulted in CQDs with increasingly indiscernible boundaries and greater overlap with neighboring nanocrystals, suggesting the degree of fusing is not a self-limiting process, but rather an effect one could exploit in a tunable fashion.

Although surface ligands are known to control CQD spacing, they also have a potentially crucial role in controlling nanoparticle fusing. This additional degree of freedom presents new design opportunities for CQD films in optimizing optoelectronic device properties. Recent studies have suggested that such fusing may lead to nanoparticle self-passivation, thus reducing the amount of effective surface area,[23] or lead to dramatic improvements in carrier mobility.[13] The major
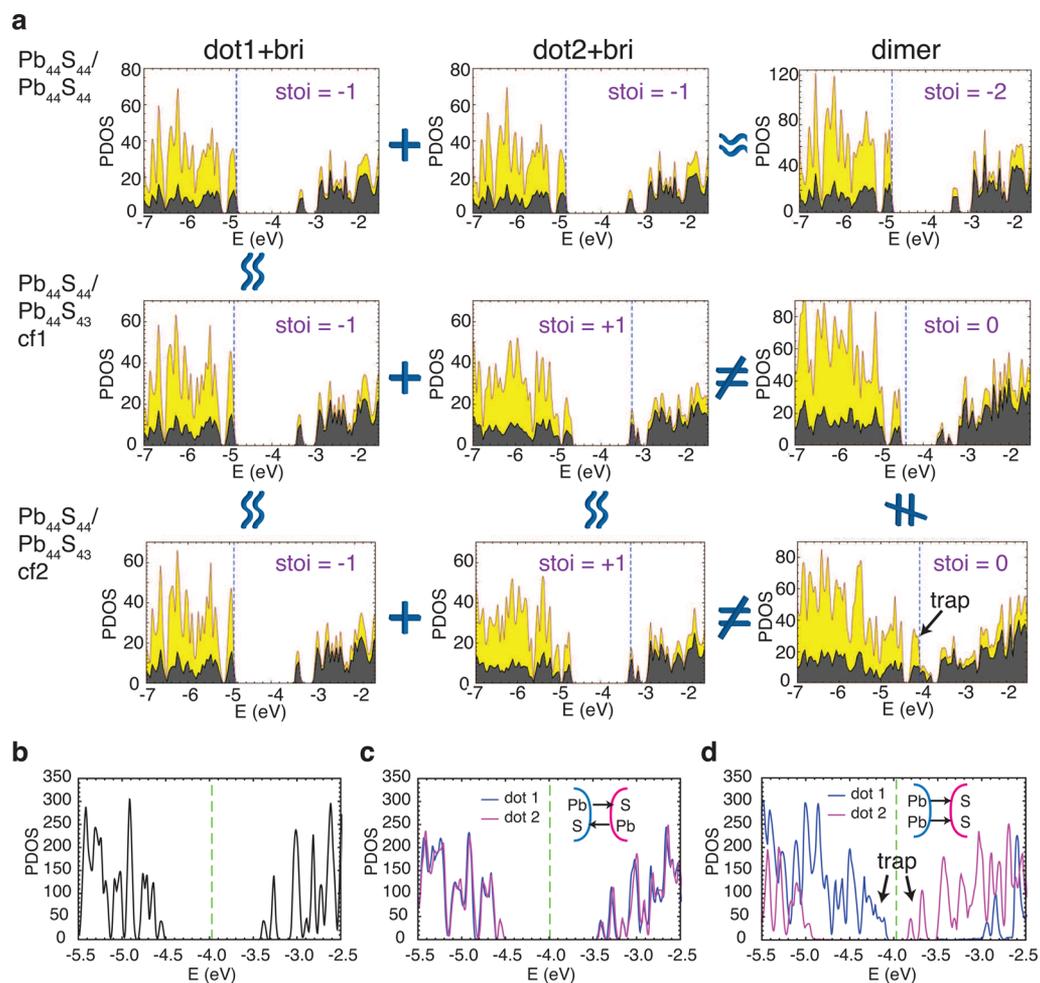
Figure 3. Connectivity-induced trap states in PbS QD dimers. (a) Comparison between PDOS on elements (Pb: gray; S: yellow) of each dot along with the bridge (1st and 2nd columns) and those of the entire system (3rd column) for the cases of $Pb_{44}S_{44}$-EDT-$Pb_{44}S_{44}$ (1st row), $Pb_{44}S_{44}$-EDT-$Pb_{44}S_{43}$ in configuration 1 (2nd row), and $Pb_{44}S_{44}$-EDT-$Pb_{44}S_{43}$ in configuration 2 (3rd row). Stoichiometry of the systems was tuned by the number of the most energetically favorable S vacancy. Configurations 1 and 2 are associated with the cases in which the S vacancy is far away from and close to the bridging site, respectively. (b) DOS of isolated $Pb_{104}S_{104}$. PDOS on each dot of $Pb_{104}S_{104}$ dimer necking *via* (c) {001} orientation and (d) {111} orientations. The vacuum level is zero, and the Fermi levels are shown in dashed lines. The horizontal arrows denote the local dipole moments from Pb to S atoms.

drawback, however, is retaining the excellent absorption and emission properties, which may be disrupted given the need to partially remove the passivating ligand shell and expose the nanocrystal core. Evidenced by the results presented here, this is an increasingly significant issue for smaller, PV-relevant particles. Furthermore, controlled fusing will be critical to the electronic energy landscape, as to prevent larger fused species, as seen for the TBAI and EDA treatments, which would suffer from a reduced energy gap, detrimental for PV device voltage.[24] Given our detailed TEM studies on PV-optimal 3 nm CQDs, it is perhaps not surprising that while thiolated organic linker treated CQDs can reach PV open-circuit voltages approaching 0.7 V,[25] the best-performing cells, which employ TBAI-treated CQDs as the photoactive layer, remain in the 0.5−0.55 V range,[22] well below their theoretical potential of 0.9 V. Even a small amount of fully fused, low-band-gap CQD cluster (1 in 100−1000) could result in substantial voltage drops due to the clusters having a much lower band gap than the polydispersity in the CQD ensemble.[24] Effectively, large size, small-band-gap clusters would result in a type-I junction with the smaller, main ensemble of CQDs, thus allowing efficient carrier shuttling into these clusters. The clusters would result in charge recombina-

tion due to low probability of escape into the higher energy CQD ensemble, where even a density of 1 in 1000 nanocrystals would result in an effective trap density of 10^{16} cm^{-3}, unacceptable for efficient photovoltaics. These low-band-gap clusters would not be reliably detected using absorption extinction coefficient measurements or photoluminescence alone, due to low concentration and limitations in detection range, respectively. Imperatively, a combination of optical and high-resolution imaging techniques must be employed to controllably engineer the next generation of partially fused CQD solids.

To complement the findings related to the different connectivity effects and defects observed in our experimental results, we develop a theoretical framework to engineering CQD solids that enables controlled necking while also revealing the importance of experimentally hard-to-access parameters. Such a formulation enables predicting the impact of necking CQDs along different crystal facets, explores the impact of fusing CQDs with a variable number of atoms, and describes the requirements necessary to preserve surface passivation and a clean band gap for high-efficiency optoelectronic devices.
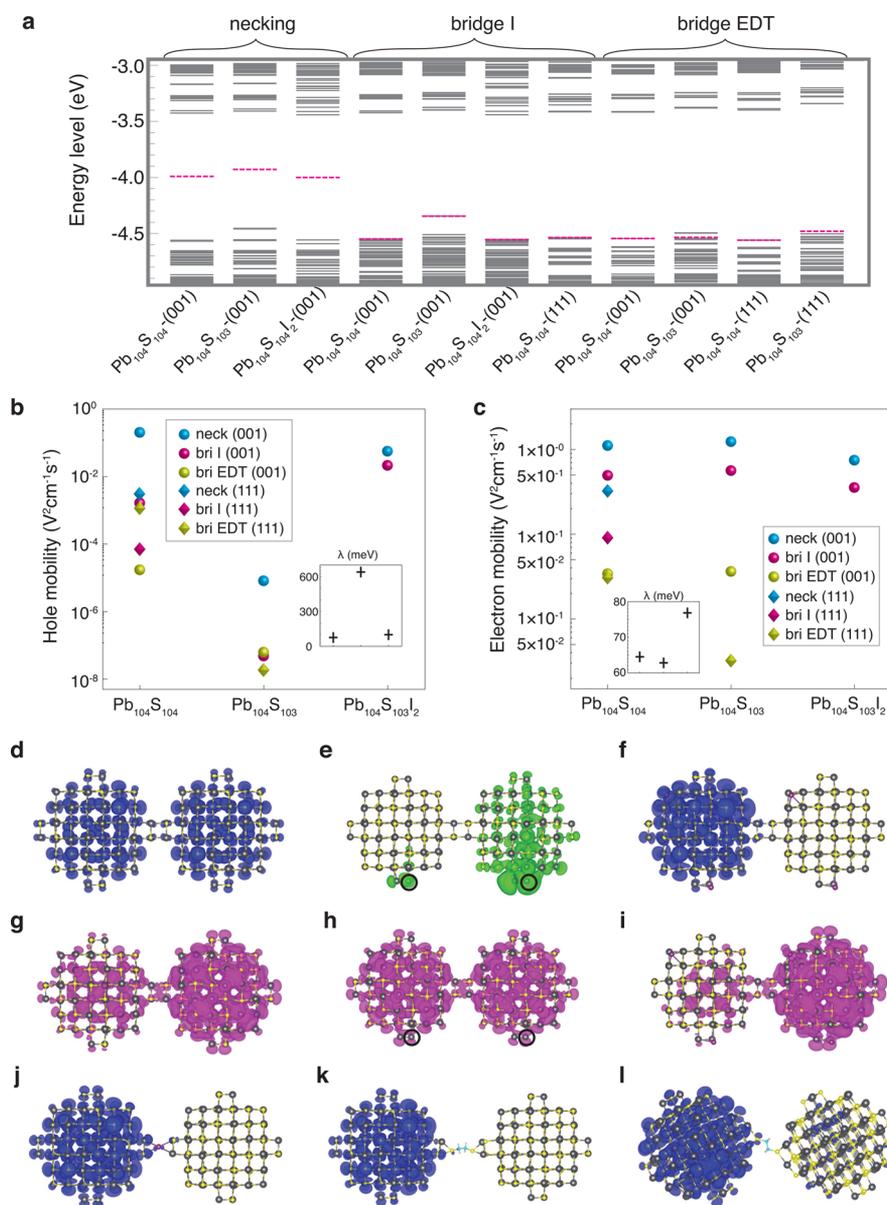
Figure 4. Impacts of connectivity on carrier mobilities. (a) Eigenvalues of $Pb_{104}S_{104}$, $Pb_{104}S_{103}$, and $Pb_{104}S_{103}I_2$ QD dimers with necking or bridging by I/EDT molecules. The Fermi levels are shown in pink dashed lines. (b) Hole and (c) electron mobilities estimated from hopping rates between connected QDs, with the corresponding reorganization energies shown in the inset figure. (The e^-/h^+ reorganization energies are 69/64, 640/63, and 92/77 meV for $Pb_{104}S_{104}$, $Pb_{104}S_{103}$, and $Pb_{104}S_{103}I_2$ respectively.) (d−f) HOMO and (g−i) LUMO wave functions of necked (d, g) $Pb_{104}S_{104}$, (e, h) $Pb_{104}S_{103}$, and (f, i) $Pb_{104}S_{103}I_2$ QD dimers. The trap state is highlighted by green color. HOMO wave functions of $Pb_{104}S_{104}$ QDs bridged by (j) I atom in {001}, (k) EDT in {001}, and (l) EDT in {111} directions.

Several theoretical studies have attempted to uncover the impact of connectivity on electronic structure,[26−29] but a major advancement in computational capabilities is still required to represent complicated realistic systems. Importantly, supperlatice models are limited in accounting for structural and energetic disorder,[26,27] while the hopping models do not account for the interface relaxation[29] or neglect the defect states.[28] Here, we develop a framework to explicitly address these issues in an attempt to build reliable connectivity models (Supplementary Section H).

CQDs with diameters $d < 5$ nm are of interest for many applications;[30−32] however, for this size range the electronic structures are highly sensitive to perturbations by the surrounding environment. In order to explore this dependence, we considered a two-dot system ($d = 1.5$ nm) connected by an EDT molecule. As shown in Figure 3a, if both dots are stoichiometric, the projected density of states (PDOS) of the combined system is similar to that of its individual components (1st row). In contrast, when one of the dots contains a S vacancy defect (2nd and 3rd rows), additional midgap trap states are introduced by bridging (3rd column) due to the hybridization between dot/bridge orbitals, and the PDOS of the combined system depends on the connectivity configuration.

Note that the importance of stoichiometry control has been demonstrated by both experimental[8,9] and theoretical studies.[17,18,33] Yet our results indicate that for comparatively small CQD assemblies global charge balance itself is not sufficient to guarantee the absence of midgap states (see the panels in Figure 3a marked by "stoi=0"). In fact, accounting for the

Table 1. Comparison between Calculated Electron/Hole Mobilities (in Units of cm² V⁻¹ s⁻¹) of Pb₁₀₄S₁₀₄ Dimers and Experimental Data

	necking		bridge I		bridge EDT	
	hole	electron	hole	electron	hole	electron
calcd {001}	2.0×10^{-1}	1.1	1.1×10^{-3}	4.9×10^{-1}	1.7×10^{-5}	3.3×10^{-2}
calcd {111}	2.2×10^{-3}	3.1×10^{-1}	7.9×10^{-5}	9.0×10^{-2}	1.1×10^{-3}	3.1×10^{-2}
exptl	$\mu_h + \mu_e = 2.6$ (13)		8.5×10^{-4} (38)	1.5×10^{-4} (38)	1×10^{-3} (36)	8×10^{-3} (36)
				1×10^{-2} (5)	1×10^{-4} (39)	2.4×10^{-4} (40)
				2.4×10^{-1} (10)		

effects of connectivity increases the challenge of eliminating midgap states, in the sense that even the simplest bridging by an I atom fails to provide a trap-free band gap for 1.5 nm CQDs. One possible approach to address this challenge is to connect QDs *via* necking rather than bridging, which effectively preserves the electronic structures of the isolated dot components (Supplementary Sections I and J, Figure S11). For relatively larger QDs with *d* = 2.1 nm, the propensity to self-heal plays a more important role, leading to a clean band gap with either an I or EDT bridge (Figure 4a, Supplementary Figure S12, Table S2).

In addition to the wave function hybridization, the shift of energy levels caused by a net dipole moment of connected dots is an important source of additional carrier traps. The origin of a dipole moment is the ionic nature of the PbS compound and asymmetric chemical environment at the interface, which can be incurred by defects, asymmetric ligands, and certain connectivity orientations. To illustrate the idea, we considered a comparatively larger CQD dimer (*d* = 2.1 nm) with three connectivity types (necking and bridging with an I atom or a EDT molecule) *via* two orientations. The results show that the dipole moment of the dot dimer is sensitive to both dot orientation and degree of connectivity (Supplementary Section J, Table S2). When the net dipole moments are close to zero, the energy levels of the dimer (Figure 3c) change slightly compared to the isolated dot (Figure 3b). In contrast, for the cases of necking *via* the {111} orientation between Pb-rich and S-rich facets, the net dipole moments are large, and potential gradients are induced in space. This causes a noticeable shift of the energy levels and a reduction of the band gap (Figure 3d, Supplementary Figure S13), which may serve as a deleterious barrier to block carrier transport as well as a potential way to achieve charge separation. A similar but less significant phenomenon is also observed on a dot dimer necking *via* {001} with a slightly asymmetric Pb/S chemical environment (Supplementary Figure S17). Such an effect may be exaggerated by employing prototype systems, since for any particular dot in the ensemble the interfacial dipoles caused by its neighbors tend to compensate each other due to the spherical symmetry. The other reason is that, in general, the {111} surface of lead chalcogenide CQD is Pb-rich, and thus it is more likely that fusion occurs between two Pb-rich {111} facets.

On the basis of the above observations, necking (fusing) would be a promising way to eliminate connectivity-induced trap states. Such a configuration is further justified by our absorption spectrum calculation; while necking between small dots (*d* = 1.5 nm) leads to a red-shift of the absorption edge, the change in a relatively large (*d* = 2.1 nm) QD dimer compared to its individual dot component is negligible (Supplementary Section K).

In addition to the energy profile, carrier mobility is another important factor in device performance. The dominant charge transfer mechanism at room temperature is phonon-assisted hopping due to the large amount of disorder in CQD assemblies.[28,34] Therefore, we explore here the influence of different bridges/neckings, connectivity orientations, carrier energies, and defect levels by computing the electron/hole hopping rates between 2.1 nm PbS QDs with Marcus theory.[35] For all cases, we employed connectivity on both the {001} and {111} facets.

We first considered the stoichiometric Pb₁₀₄S₁₀₄ dimer (1st column of Figure 4b,c). As summarized in Table 1, our calculated carrier mobilities are, in general, consistent with experimental data and correctly reproduce two general trends: (1) electron mobilities are much higher than hole mobilities,[36,37] which can be explained by the more extended LUMO (Figure 4g) than HOMO (Figure 4d) wavefuction; (2) necking leads to much more efficient charge transport compared to bridging with small molecules,[13] which is attributed to the stronger electron coupling induced by the larger overlap between relevant orbitals. For our purpose of probing the general impact of dot communication, such qualitative agreement within the trends is sufficient. Beside employing the correct CQD size, improved agreement could be achieved by accounting for any small amount of necking that may exist in the CQD assemblies with short bridges,[7] the distributions of size/configuration, the contributions from hot states (Supplementary Section L), and the influence of trap states (which were ignored for our current simulations). Note that the carrier mobilities of bridged CQDs depend strongly on the connection facets, due to the sensitivity of electron coupling to the orbital hybridization and dot-to-dot distance (Supplementary Section M).

On the basis of our simulations, necking *via* the {001} direction seems to be the most promising connectivity for high carrier mobility, which can be achieved by standard ligand exchange techniques to fuse CQDs, because the binding energy of OA ligands on the {001} surface was shown to be weaker than that on the {111} surface by previous theoretical studies.[41] To investigate the influence of degree of necking on electron coupling, we considered 2.3 nm PbS dot dimers containing relatively large {001} facets. While, in general, the electron coupling increases with increasing degree of necking, which is consistent with previous tight-binding calculations,[26,27] it could also be substantially affected by the local chemical environment. Thus, the width of the neck should be sufficiently large to cover the sites with large overlap between wave functions (Supplementary Section N).

As a prototype system, we explored the communications between two slightly off-stoichiometric Pb₁₀₄S₁₀₃ dots with S vacancy, which introduces trap states (Figure 4e) near the HOMO level (Figure 4a). While the electron mobilities are

barely affected, the hole mobilities dramatically drop by 2 to 4 orders of magnitude regardless of the connectivity type, consistent with the much higher carrier mobilities of band-edge states than those of midgap states as observed in experiment.[42] Such deleterious effects of trap states are consequences of both weakened electron couplings between localized wave functions and a much larger reorganization energy that increases the effective hopping barriers (inset of Figure 4d).

One practical solution to mitigate trap states caused by the S vacancy is passivation of defects by atomic halide ligands.[2,3,5] When we attached two I ligands to each of the $Pb_{104}S_{103}$ dots, the reorganization energy becomes similar to the ideal $Pb_{104}S_{104}$ dot, and the wave functions are once again delocalized (Figure 4f), leading to a recovery of the hole mobility to 5.5×10^{-2} cm^2 V^{-1} s^{-1} for necked QDs. Since the exact number of attached I ligands is difficult to control, one may be concerned that excessive I ligands could introduce other types of trap states. We tested this hypothesis and found that neither the reorganization energy nor wave function delocalization is sensitive to additional I ligands (Supplementary Section O). The above analysis implies that one strategy to enhance carrier mobilities is first connecting CQDs by necking and then passivating defects by atomic ligands.

Again, a key conclusion that can be drawn from these calculations is that the role of connectivity between dots is crucial in order to understand thin-film performance and properties. CQD films cannot always be computationally represented as a collection of isolated dots, as both important deleterious effects and opportunities for improved designs will be missed.

We note that our computational results should be interpreted qualitatively, as the prototype systems in our simulations are somewhat different from the realistic case of PbS CQDs for current solar cells. While both stoichiometric and slightly off-stoichiometric CQDs were considered in our simulations, experimentally CQDs treated with a variety of ligands rarely result in stoichiometric (intrinsic) nanocrystals, where both the core and ligand species are required to assess the exact stoichiometry.[18] However, such a deviation will not cause qualitative differences in transport properties of intrinsic states that are relevant to typical mobility measurement in transistors, as the calculated wave functions of intrinsic states in off-stoichiometric QDs are similar to those in stoichiometric QDs (Supplementary Section P).

Another source of deviation from practical conditions is that the prototype systems used in our simulations are smaller than those typically used in experiments. Fortunately, the comparison of our calculated PDOS for 2.1 nm QDs (Figure S12) to those reported for 4 nm PbS QDs in previous computational studies[43] suggests that our prototype systems are sufficient to represent the electronic structure of realistic QDs. In addition, the QDs containing defects in this work exhibit localized HOMO wave functions on the surface, which are similar to the localized orbitals of in-gap states on 4 nm PbS QDs.[43] However, predicting the variation of carrier mobility with respect to QD size is quite challenging, because two key factors of carrier transport, the reorganization energy and electronic coupling, have distinct dependence on QD size.[28] In this sense, no simple extrapolation is feasible to quantitatively predict the carrier mobility for larger QDs; yet we expect that the connectivity strategies obtained by our small QDs are still valid for larger QDs. That is because the differences in mobility between various connectivity motifs mainly arise from the differences in electron coupling, and wave function shapes are insensitive to the QD size (Supplementary Section P).

CONCLUSION

Both the experimental and theoretical results reveal that controlling the specific effects arising from connectivity of CQDs is essential for generating highly efficient CQD solid films. We find that ligand treatment morphologies can vary dramatically depending on ligand choice and concentration and that previously thought to be benign treatment can lead to potentially detrimental electronic defects within CQD opto-electric films. The basis formed by our experimental results is further complemented by computational models that go beyond the single-CQD picture, revealing yet another set of design criteria for CQD solids. For small dots, both necking and bridging with small molecules could change the electronic structure substantially, mandating control over the interface structure beyond stoichiometry is necessary to eliminate trap states and to reduce the emission line width. We show that carrier mobility in these structures depends not only on separation but also on choice of ligand itself, connectivity orientation, carrier energy, and defect states. Taken together, we present a novel approach to generating highly efficient CQD solids by initial necking of nanocrystals followed by excess atomic ligand passivation. We have shown that moving beyond the realm of single-CQD simulation will be important for both the fundamental understanding and engineering of novel CQD materials and shed light on the connectivity designs that open opportunities toward highly efficient optoelectronic devices.

METHODS

CQD Synthesis. PbS CQDs were synthesized according to a modified literature recipe.[44] PbS CQDs of 3 nm were synthesized by heating 0.45 g of PbO (Alfa Aesar) with 1.5 mL of oleic acid (Sigma) in 18 mL of octadecene (Alfa Aesar) in an oil bath at 100 °C under a vacuum of <1 mbar. After 2 h, the temperature was lowered to 80 °C and the reaction was exposed to nitrogen gas, and 20 μL of TMS (Sigma) in 10 mL of ODE was injected into the flask while purging with nitrogen. The heating was immediately turned off, and the reaction was allowed to cool to 30 °C in the oil bath before isolation in acetone. For 8 nm CQD synthesis, 0.18 g of PbO was utilized with 8 mL of OA and 84 μL of TMS in 4 mL of ODE. The injection temperature was 150 °C. The CQD cleaning procedure involved precipitating the nanocrystals in acetone twice, redissolving in toluene, followed by centrifugation at 12 krpm for 2 min, and taking the supernatant. CQD batches used for each type of dot size were kept consistent throughout all experiments.

TEM Sample Preparation and Imaging. CQDs were drop cast onto amorphous carbon TEM grids (Electron Microscopy Sciences) at concentrations of 1−5 mg/mL. An underlying filter paper was used to whisk away excess solution from the grid. Ligand exchange was carried out at 0.05−1 M concentrations by dip-coating the samples for <30 s into a ligand−methanol solution. The ligand concentration for Figure 2 was chosen for TBAI in accordance with processing of CQD films for photovoltaic applications (10 mg/mL).[21] All other ligand concentrations were adjusted to study the ligand effect only. The grid was then rinsed with methanol over filter paper before imaging. Images were acquired on a JEOL JEM 2100.

PbS CQD Film Fabrication. CQDs were deposited at a concentration of 50 mg/mL (in octane) and spun at 2500 rpm onto a glass substrate. Ligand treatments were administered according to the preparation outlined in the TEM studies. Two methanol rinses were administered between layers. The final sample thickness was approximately 150 nm (five layers).

Absorption Measurements. Absorption was carried out using a Cary 5000 spectrophotometer.

Simulation on CQD Dimers. Three different sizes of PbS QDs (1.5, 2.1, and 2.3 nm in diameter) were prepared by carving a sphere from bulk crystals. Slightly off-stoichiometric dots were used as representatives to introduce trap states near the highest occupied molecular orbital (HOMO). We carried out standard *ab initio* calculations within the DFT framework, using the Vienna Ab Initio Simulation Package (VASP, v5.3).[45] Plane-wave and projector-augmented-wave (PAW)-type pseudopotentials[46] with kinetic-energy cutoffs of up to 400 eV were employed, along with the PBE exchange–correlation functional.[47] To obtain electron couplings between dots, we applied the anticrossing method,[28] with eigenvalues perturbed by external electric fields obtained by the SIESTA (v3.2) package.[48] A polarized double-ζ basis set[49] was used for the localized numerical atomic orbitals.[50] The relativistic Troullier–Martins pseudopotentials with nonlinear core corrections[51] and the PBE exchange–correlation functional[47] were employed. The phonon-assisted charge-hopping rates were computed using Marcus theory,[35] which has been widely used to understand charge dynamics in organic systems,[52,53] but was applied to only a few QD systems due to the computational difficulty.[28,29,54,55] Although Marcus theory does not account for quantum tunneling effects, it yields reasonable results provided that the driving forces are close to zero.[28,54] Finally, the absorption spectra were calculated with the random phase approximation by the BerkeleyGW (v1.1)[56] and the Quantum Espresso (v5.0.3)[57] packages. Further details regarding the computational methods are provided in Supplementary Section H.

ASSOCIATED CONTENT

Ⓢ Supporting Information

The Supporting Information is available free of charge on the ACS Publications website at DOI: 10.1021/acsnano.5b05626.

    Additional figures and details as described in the text (PDF)

AUTHOR INFORMATION

Corresponding Author
*E-mail (J. C. Grossman): jcg@mit.edu.

Author Contributions
‡H. Li and D. Zhitomirsky contributed equally to this work.

Notes
The authors declare no competing financial interest.

ACKNOWLEDGMENTS

REFERENCES

(1) Talapin, D. V.; Lee, J.-S.; Kovalenko, M. V.; Shevchenko, E. V. Prospects of Colloidal Nanocrystals for Electronic and Optoelectronic Applications. *Chem. Rev.* **2009**, *110*, 389−458.

(2) Ip, A. H.; Thon, S. M.; Hoogland, S.; Voznyy, O.; Zhitomirsky, D.; Debnath, R.; Levina, L.; Rollny, L. R.; Carey, G. H.; Fischer, A.; et al. Hybrid Passivated Colloidal Quantum Dot Solids. *Nat. Nanotechnol.* **2012**, *7*, 577−582.

(3) Katsiev, K.; Ip, A. H.; Fischer, A.; Tanabe, I.; Zhang, X.; Kirmani, A. R.; Voznyy, O.; Rollny, L. R.; Chou, K. W.; Thon, S. M.; et al. The Complete In-Gap Electronic Structure of Colloidal Quantum Dot Solids and Its Correlation with Electronic Transport and Photovoltaic Performance. *Adv. Mater.* **2014**, *26*, 937−942.

(4) Thon, S. M.; Ip, A. H.; Voznyy, O.; Levina, L.; Kemp, K. W.; Carey, G. H.; Masala, S.; Sargent, E. H. Role of Bond Adaptability in the Passivation of Colloidal Quantum Dot Solids. *ACS Nano* **2013**, *7*, 7680−7688.

(5) Tang, J.; Kemp, K. W.; Hoogland, S.; Jeong, K. S.; Liu, H.; Levina, L.; Furukawa, M.; Wang, X.; Debnath, R.; Cha, D.; et al. Colloidal-Quantum-Dot Photovoltaics Using Atomic-ligand Passivation. *Nat. Mater.* **2011**, *10*, 765−771.

(6) Rath, A.; Pelayo Garcia de Arquer, F.; Stavrinadis, A.; Lasanta, T.; Bernechea, M.; Diedenhofen, S. L.; Konstantatos, G. Remote Trap Passivation in Colloidal Quantum Dot Bulk Nano-Heterojunctions and Its Effect in Solution-Processed Solar Cells. *Adv. Mater.* **2014**, *26*, 4741−4747.

(7) Liu, Y.; Tolentino, J.; Gibbs, M.; Ihly, R.; Perkins, C. L.; Liu, Y.; Crawford, N.; Hemminger, J. C.; Law, M. PbSe Quantum Dot Field-Effect Transistors with Air-Stable Electron Mobilities above 7 cm2 V-1 s-1. *Nano Lett.* **2013**, *13*, 1578−1587.

(8) Engel, J. H.; Alivisatos, A. P. Postsynthetic Doping Control of Nanocrystal Thin Films: Balancing Space Charge to Improve Photovoltaic Efficiency. *Chem. Mater.* **2013**, *26*, 153−162.

(9) Luther, J. M.; Pietryga, J. M. Stoichiometry Control in Quantum Dots: A Viable Analog to Impurity Doping of Bulk Materials. *ACS Nano* **2013**, *7*, 1845−1849.

(10) Ning, Z.; Ren, Y.; Hoogland, S.; Voznyy, O.; Levina, L.; Stadler, P.; Lan, X.; Zhitomirsky, D.; Sargent, E. H. All-Inorganic Colloidal Quantum Dot Photovoltaics Employing Solution-Phase Halide Passivation. *Adv. Mater.* **2012**, *24*, 6295−6299.

(11) Gao, Y.; Aerts, M.; Sandeep, C. S.; Talgorn, E.; Savenije, T. J.; Kinge, S.; Siebbeles, L. D.; Houtepen, A. J. Photoconductivity of PbSe Quantum-Dot Solids: Dependence on Ligand Anchor Group and Length. *ACS Nano* **2012**, *6*, 9606−9614.

(12) Liu, W.; Lee, J.-S.; Talapin, D. V. III-V Nanocrystals Capped with Molecular Metal Chalcogenide Ligands: High Electron Mobility and Ambipolar Photoresponse. *J. Am. Chem. Soc.* **2013**, *135*, 1349−1357.

(13) Sandeep, C. S.; Azpiroz, J. M.; Evers, W. H.; Boehme, S. C.; Moreels, I.; Kinge, S.; Siebbeles, L. D.; Infante, I.; Houtepen, A. J. Epitaxially Connected PbSe Quantum-Dot Films: Controlled Neck Formation and Optoelectronic Properties. *ACS Nano* **2014**, *8*, 11499−11511.

(14) Baumgardner, W. J.; Whitham, K.; Hanrath, T. Confined-but-Connected Quantum Solids via Controlled Ligand Displacement. *Nano Lett.* **2013**, *13*, 3225−3231.

(15) Boneschanscher, M.; Evers, W.; Geuchies, J.; Altantzis, T.; Goris, B.; Rabouw, F.; van Rossum, S.; van der Zant, H.; Siebbeles, L.; Van Tendeloo, G. Long-Range Orientation and Atomic Attachment of Nanocrystals in 2D Honeycomb Superlattices. *Science* **2014**, *344*, 1377−1380.

(16) Boles, M. A.; Talapin, D. V. Connecting the Dots. *Science* **2014**, *344*, 1340−1341.

(17) Kim, D.; Kim, D.-H.; Lee, J.-H.; Grossman, J. C. Impact of Stoichiometry on the Electronic Structure of PbS Quantum Dots. *Phys. Rev. Lett.* **2013**, *110*, 196802.

(18) Voznyy, O.; Zhitomirsky, D.; Stadler, P.; Ning, Z.; Hoogland, S.; Sargent, E. H. A Charge-Orbital Balance Picture of Doping in Colloidal Quantum Dot Solids. *ACS Nano* **2012**, *6*, 8448−8455.

(19) Brown, P. R.; Kim, D.; Lunt, R. R.; Zhao, N.; Bawendi, M. G.; Grossman, J. C.; Bulovic, V. Energy Level Modification in Lead Sulfide Quantum Dot Thin Films through Ligand Exchange. *ACS Nano* **2014**, *8*, 5863−5872.

(20) Weidman, M. C.; Yager, K. G.; Tisdale, W. A. Interparticle Spacing and Structural Ordering in Superlattice PbS Nanocrystal Solids Undergoing Ligand Exchange. *Chem. Mater.* **2015**, *27*, 474−482.

(21) Zhitomirsky, D.; Furukawa, M.; Tang, J.; Stadler, P.; Hoogland, S.; Voznyy, O.; Liu, H.; Sargent, E. H. N-Type Colloidal-Quantum-Dot Solids for Photovoltaics. *Adv. Mater.* **2012**, *24*, 6181−6185.

(22) Chuang, C.-H. M.; Brown, P. R.; Bulović, V.; Bawendi, M. G. Improved Performance and Stability in Quantum Dot Solar Cells through Band Alignment Engineering. *Nat. Mater.* **2014**, *13*, 796−801.

(23) Carey, G. H.; Levina, L.; Comin, R.; Voznyy, O.; Sargent, E. H. Record Charge Carrier Diffusion Length in Colloidal Quantum Dot Solids *via* Mutual Dot-To-Dot Surface Passivation. *Adv. Mater.* **2015**, *27*, 3325.

(24) Zhitomirsky, D.; Kramer, I. J.; Labelle, A. J.; Fischer, A.; Debnath, R.; Pan, J.; Bakr, O. M.; Sargent, E. H. Colloidal Quantum Dot Photovoltaics: the Effect of Polydispersity. *Nano Lett.* **2012**, *12*, 1007−1012.

(25) Zhitomirsky, D.; Voznyy, O.; Levina, L.; Hoogland, S.; Kemp, K. W.; Ip, A. H.; Thon, S. M.; Sargent, E. H. Engineering Colloidal Quantum Dot Solids Within and Beyond the Mobility-Invariant Regime. *Nat. Commun.* **2014**, 510.1038/ncomms4803.

(26) Kalesaki, E.; Evers, W.; Allan, G.; Vanmaekelbergh, D.; Delerue, C. Electronic Structure of Atomically Coherent Square Semiconductor Superlattices with Dimensionality below Two. *Phys. Rev. B: Condens. Matter Mater. Phys.* **2013**, *88*, 115431.

(27) Kalesaki, E.; Delerue, C.; Smith, C. M.; Beugeling, W.; Allan, G.; Vanmaekelbergh, D. Dirac Cones, Topological Edge States, and Nontrivial Flat Bands in Two-Dimensional Semiconductors with a Honeycomb Nanogeometry. *Phys. Rev. X* **2014**, *4*, 011010.

(28) Chu, I.-H.; Radulaski, M.; Vukmirovic, N.; Cheng, H.-P.; Wang, L.-W. Charge Transport in a Quantum Dot Supercrystal. *J. Phys. Chem. C* **2011**, *115*, 21409−21415.

(29) Kaushik, A. P.; Lukose, B.; Clancy, P. The Role of Shape on Electronic Structure and Charge Transport in Faceted PbSe Nanocrystals. *ACS Nano* **2014**, *8*, 2302−2317.

(30) Shirasaki, Y.; Supran, G. J.; Bawendi, M. G.; Bulović, V. Emergence of Colloidal Quantum-Dot Light-Emitting Technologies. *Nat. Photonics* **2013**, *7*, 13−23.

(31) Lin, Z.; Franceschetti, A.; Lusk, M. T. Size Dependence of the Multiple Exciton Generation Rate in CdSe Quantum Dots. *ACS Nano* **2011**, *5*, 2503−2511.

(32) Lin, Z.; Li, H.; Franceschetti, A.; Lusk, M. T. Efficient Exciton Transport between Strongly Quantum-confined Silicon Quantum Dots. *ACS Nano* **2012**, *6*, 4029−4038.

(33) Grassi, F.; Argeri, M.; Marchese, L.; Cossi, M. First Principle Study of Capping Energies and Electronic States in Stoichiometric and Nonstoichiometric PbSe Nanoclusters. *J. Phys. Chem. C* **2013**, *117*, 26396−26404.

(34) Guyot-Sionnest, P. Electrical Transport in Colloidal Quantum Dot Films. *J. Phys. Chem. Lett.* **2012**, *3*, 1169−1175.

(35) Marcus, R. A. Electron Proton and Related Transfers. *Faraday Discuss. Chem. Soc.* **1982**, *74*, 7−15.

(36) Osedach, T. P.; Zhao, N.; Andrew, T. L.; Brown, P. R.; Wanger, D. D.; Strasfeld, D. B.; Chang, L.-Y.; Bawendi, M. G.; Bulovic, V. Bias-Stress Effect in 1, 2-ethanedithiol-Treated PbS Quantum Dot Field-Effect Transistors. *ACS Nano* **2012**, *6*, 3121−3127.

(37) Liu, Y.; Gibbs, M.; Puthussery, J.; Gaik, S.; Ihly, R.; Hillhouse, H. W.; Law, M. Dependence of Carrier Mobility on Nanocrystal Size and Ligand Length in PbSe Nanocrystal Solids. *Nano Lett.* **2010**, *10*, 1960−1969.

(38) Wanger, D. D.; Correa, R. E.; Dauler, E. A.; Bawendi, M. G. The Dominant Role of Exciton Quenching in PbS Quantum-Dot-Based Photovoltaic Devices. *Nano Lett.* **2013**, *13*, 5907−5912.

(39) Klem, E. J.; Shukla, H.; Hinds, S.; MacNeil, D. D.; Levina, L.; Sargent, E. H. Impact of Dithiol Treatment and Air Annealing on the Conductivity, Mobility, and Hole Density in PbS Colloidal Quantum Dot Solids. *Appl. Phys. Lett.* **2008**, *92*, 212105.

(40) Jeong, K. S.; Tang, J.; Liu, H.; Kim, J.; Schaefer, A. W.; Kemp, K.; Levina, L.; Wang, X.; Hoogland, S.; Debnath, R.; et al. Enhanced Mobility-Lifetime Products in PbS Colloidal Quantum Dot Photovoltaics. *ACS Nano* **2011**, *6*, 89−99.

(41) Zherebetskyy, D.; Scheele, M.; Zhang, Y.; Bronstein, N.; Thompson, C.; Britt, D.; Salmeron, M.; Alivisatos, P.; Wang, L.-W. Hydroxylation of the Surface of PbS Nanocrystals Passivated with Oleic Acid. *Science* **2014**, *344*, 1380−1384.

(42) Nagpal, P.; Klimov, V. I. Role of Mid-Gap States in Charge Transport and Photoconductivity in Semiconductor Nanocrystal Films. *Nat. Commun.* **2011**, *2*, 486.

(43) Zhang, Y.; Zherebetskyy, D.; Bronstein, N. D.; Barja, S.; Lichtenstein, L.; Alivisatos, A. P.; Wang, L.-W.; Salmeron, M. Molecular Oxygen Induced In-Gap States in PbS Quantum Dots. *ACS Nano* **2015**, *9*, 10445−10452.

(44) Hines, M. A.; Scholes, G. D. Colloidal PbS Nanocrystals with Size-Tunable Near-infrared Emission: Observation of Post-Synthesis Self-Narrowing of the Particle Size Distribution. *Adv. Mater.* **2003**, *15*, 1844−1849.

(45) Kresse, G.; Furthmüller, J. Efficient Iterative Schemes for Ab Initio Total-Energy Calculations Using a Plane-Wave Basis Set. *Phys. Rev. B: Condens. Matter Mater. Phys.* **1996**, *54*, 11169.

(46) Blöchl, P. E. Projector Augmented-Wave Method. *Phys. Rev. B: Condens. Matter Mater. Phys.* **1994**, *50*, 17953.

(47) Perdew, J. P.; Burke, K.; Ernzerhof, M. Generalized Gradient Approximation Made Simple. *Phys. Rev. Lett.* **1996**, *77*, 3865.

(48) Soler, J. M.; Artacho, E.; Gale, J. D.; García, A.; Junquera, J.; Ordejón, P.; Sánchez-Portal, D. The SIESTA Method for Ab initio Order-N Materials Simulation. *J. Phys.: Condens. Matter* **2002**, *14*, 2745.

(49) Junquera, J.; Paz, Ó; Sánchez-Portal, D.; Artacho, E. Numerical Atomic Orbitals for Linear-Scaling Calculations. *Phys. Rev. B: Condens. Matter Mater. Phys.* **2001**, *64*, 235111.

(50) Voznyy, O.; Thon, S.; Ip, A.; Sargent, E. Dynamic Trap Formation and Elimination in Colloidal Quantum Dots. *J. Phys. Chem. Lett.* **2013**, *4*, 987−992.

(51) Troullier, N.; Martins, J. L. Efficient Pseudopotentials for Plane-Wave Calculations. *Phys. Rev. B: Condens. Matter Mater. Phys.* **1991**, *43*, 1993.

(52) Jortner, J. Temperature Dependent Activation Energy for Electron Transfer between Biological Molecules. *J. Chem. Phys.* **1976**, *64*, 4860−4867.

(53) Yi, Y.; Coropceanu, V.; Brédas, J.-L. Exciton-Dissociation and Charge-Recombination Processes in Pentacene/C60 Solar Cells: Theoretical Insight into the Impact of Interface Geometry. *J. Am. Chem. Soc.* **2009**, *131*, 15777−15783.

(54) Li, H.; Wu, Z.; Lusk, M. T. Dangling Bond Defects: The Critical Roadblock to Efficient Photoconversion in Hybrid Quantum Dot Solar Cells. *J. Phys. Chem. C* **2013**, *118*, 46−53.

(55) Li, H.; Wu, Z.; Zhou, T.; Sellinger, A.; Lusk, M. T. Double Superexchange in Quantum Dot Mesomaterials. *Energy Environ. Sci.* **2014**, *7*, 1023−1028.

(56) Deslippe, J.; Samsonidze, G.; Strubbe, D. A.; Jain, M.; Cohen, M. L.; Louie, S. G. BerkeleyGW: A Massively Parallel Computer Package for the Calculation of the Quasiparticle and Optical Properties of Materials and Nanostructures. *Comput. Phys. Commun.* **2012**, *183*, 1269−1289.

(57) Giannozzi, P.; Baroni, S.; Bonini, N.; Calandra, M.; Car, R.; Cavazzoni, C.; Ceresoli, D.; Chiarotti, G. L.; Cococcioni, M.; Dabo, I.; et al. QUANTUM ESPRESSO: a Modular and Open-Source Software Project for Quantum Simulations of Materials. *J. Phys.: Condens. Matter* **2009**, *21*, 395502.